RI 7699

Bureau of Mines Report of Investigations/1972

Experimental Investigations of an Open-Cycle, Vortex MHD Generator

UNITED STATES DEPARTMENT OF THE INTERIOR

Report of Investigations 7699

Experimental Investigations of an Open-Cycle, Vortex MHD Generator

By George J. Conroy, Roy C. Kurtzrock, Richard B. Snedden, Joseph J. Demeter, Daniel Bienstock, and William F. Hughes
Pittsburgh Energy Research Center, Pittsburgh, Pa.

UNITED STATES DEPARTMENT OF THE INTERIOR
Rogers C. B. Morton, Secretary

BUREAU OF MINES
Elburt F. Osborn, Director

This publication has been cataloged as follows:

Conroy, George J

Experimental investigations of an open-cycle, vortex MHD generator, by George J. Conroy [and others. Washington] U.S. Dept. of the Interior, Bureau of Mines [1972]

28 p. illus., tables. (U.S. Bureau of Mines. Report of investigations 7699)

Includes bibliography.

1. Vortex generators. 2. Magnetohydrodynamic generators. 3. Electric power production. I. Title. (Series)

TN23.U7 no. 7699 622.06173

U.S. Dept. of the Int. Library

CONTENTS

ILLUSTRATIONS

TABLES

EXPERIMENTAL INVESTIGATIONS OF AN OPEN-CYCLE, VORTEX MHD GENERATOR

by

George J. Conroy,[1] Roy C. Kurtzrock,[2] Richard B. Snedden,[2] Joseph J. Demeter,[2]
Daniel Bienstock,[2] and William F. Hughes[3]

ABSTRACT

Electrical power generation was studied in a laboratory-scale, open-cycle vortex MHD generator, which offers several advantages over straight-channel generators that require separate combustors. Compactness, lower capital cost, and high-energy release are obtained by combining the combustor and generator into one unit in the vortex generator. In addition, the vortex generator uses a simple solenoid rather than the more complex and expensive saddle magnet required for straight-channel generators.

Although the vortex generator must utilize combustion gases with a low Hall coefficient in order to be efficient in direct comparison to the linear generator, the primary motivation for this experimental device in terms of ultimate objective was to investigate the vortex generator with applications to direct coal firing and with combustion taking place in specially designed expansion nozzles. The vortex device offers one decided advantage over the linear device in this regard because slag deposits do not degrade or short-circuit the coaxial electrodes as is the case for a linear machine.

The experimental vortex generator consists of a modified cyclone burner 7½ in ID by 21 in long, with the inner wall used as one electrode together with a coaxial center electrode. Power was obtained by impressing an axial field of 3,000 G from an air core solenoid magnet. Tests were conducted by seeding natural gas seeded with potassium acetate and burning with preheated oxygen-enriched air. Power generation was lower than calculated because theoretical plasma velocities were not achieved.

INTRODUCTION

In a vortex MHD generator, a rotating stream of hot conductive gases travels through a magnetic field which is oriented along the axis of rotation of the gas. Radial movement of free electrons is thereby induced, constituting

---

[1] Electrical research engineer.
[2] Chemical research engineer.
[3] Mechanical engineer (faculty member, Carnegie-Mellon University, Pittsburgh, Pa.).

a generated electrical current between the inner wall of the circular chamber used as one electrode and a coaxial center electrode. Although open-cycle MHD development has been almost exclusively concerned with use of straight-channel generators requiring separate combustors, vortex generators offer several advantages. By combining the combustor, nozzle, and generator into one unit, compactness, lower capital cost, and high-energy release are obtained. Vortex generation also offers low wall friction and heat losses, lower sensitivity to ash deposits, greater interaction length than straight generators of comparable volume, and use of a simple solenoid rather than the more complex and expensive saddle magnet. Similarly, the high-power-density disk generator operating at high Hall coefficients together with the simpler channel and magnet system indicates a potential engineering advantage of the disk over linear configurations.

If coal is used directly as a fuel, the slag deposits tend to degrade and short out the electrodes in either a Hall- or Faraday-type linear generator. The primary motivation of this study was to investigate the vortex generator with the solving of the slag problem as the ultimate objective. Because of the necessary low Hall coefficient to minimize losses in the vortex device, the direct comparison of gas-fired linear and vortex generator is not simple and depends on many parameters. In general, the linear Hall machine is probably superior. However, if coal is to be used as a fuel, the vortex device seems to offer several inherent advantages: the possibility of allowing at least partial combustion in specially designed swirl nozzles and partially in the vortex itself, and the fact that slag deposits do not short out the electrodes in a vortex device.

Although coal was not actually burned in these tests, the general theory and several materials problems were studied.

Theoretical analyses of vortex generators have been confined to studies of the one-dimensional flow problem where the velocity depends only on the radial coordinates. In this thin disklike configuration, the flow can be analyzed for inward or outward spiraling motion, and the electrodes can be either concentric cylinders or flat parallel plates. In this paper, the two-dimensional flow problem is considered where the velocity depends on both radial and axial coordinates.

To test the vortex MHD principle with an actual combustion system, a modified cyclone burner was designed and built in which natural gas seeded with potassium acetate was burned with preheated oxygen-enriched air at a thermal input of 0.4 Mw. An axial magnetic field of 3,000 G was impressed upon this system during power generation tests. This report presents the theoretical analysis of the generator and summarizes the results of the power generation experiments.

THEORETICAL ANALYSIS

In a cylindrical chamber, if gas is introduced tangentially at one end, at high velocity, it will spiral over a considerable depth before exiting through a port in the opposite end wall. The rotational velocity of any free

electrons (charged particles) in the gas stream will interact with an applied magnetic field, which is oriented along the axis of the spiral, causing a force on the free electrons, and thereby resulting in a radial electron flow in the chamber. If electrodes are placed at the axis and outer wall of the chamber and connected through an external load, an electric circuit will be completed and the construction will form a "vortex" MHD generator.

The vortex MHD construction theoretically offers low wall friction, low heat loss, and short actual length for a given reaction length. Also, since the magnet coil required is a solenoid rather than the physically weaker and more complex saddle magnet of the linear MHD generator, the exterior structure is smaller and less complex. For these reasons, the vortex principle was considered worthy of investigation, on a reduced-scale-model basis, for its applicability to a coal-fired MHD generator. In the model generator, the energy utilized to provide the high tangential velocity was that energy added to the combustion air through compression and preheat. Combustion took place in the chamber to increase the gas conductivity rather than to provide the kinetic energy to be converted to electrical energy. In a practical device, the generator would be designed so that the combustion energy contributed to the tangential velocity and, therefore, to the power generation.

Theoretical analysis of the present configuration requires consideration of a two-dimensional flow problem wherein the velocity depends on both radial and axial coordinates. The geometry of the system, in cylindrical coordinates, is as shown in figure 1. Figure 2 shows the equivalent circuit. Mathematical derivations developed during the initial phase of this project are included in appendix A. The assumptions and derived performance equations are repeated below for convenience.

Assumptions:

(a) The gas is inviscid, and boundary layer effects are confined to a thin layer along the electrode surfaces. Effects of secondary flow due to the viscosity are neglected.

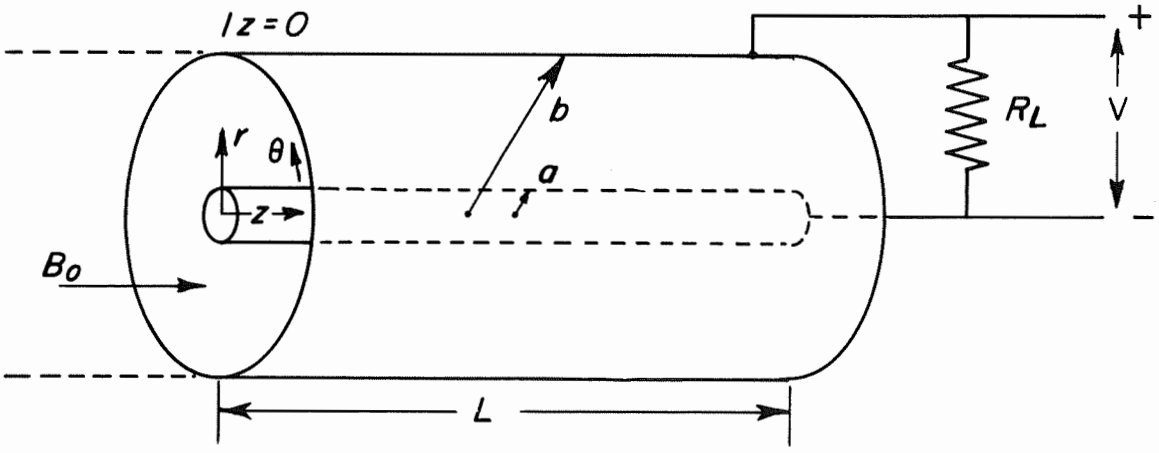

FIGURE 1. - Axial-Field Vortex MHD Generator.

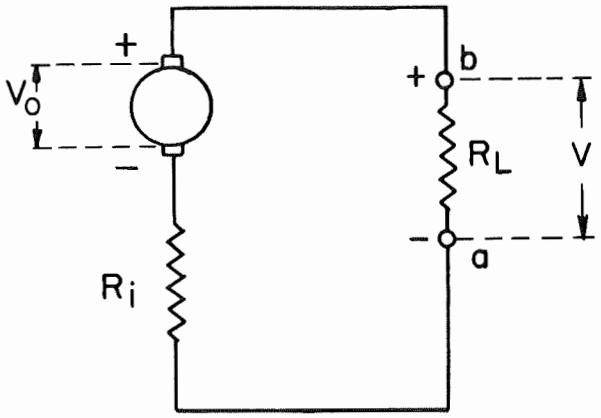

FIGURE 2. - Equivalent Circuit of the Generator.

(b) The radial velocity is negligible compared with the tangential velocity.

(c) The flow is axially symmetric; that is, all quantities are independent of θ.

(d) The magnetic Reynold's number is small so that the applied magnetic field, B_o, is essentially unchanged, and induced fields can be neglected.

(e) The flow is in steady state.

(f) The conductivity of the electrodes is much greater than that of the gas, so that the axial component of the electric field in the electrodes is zero.

(g) E_r is independent of z; that is, $E_r = E_r(r)$.

Equations obtained:

Tangential velocity:

$$U_\theta = U_\theta^\circ(r) - \frac{I B_o}{2\pi r \rho U_z} \cdot \frac{\Psi(z)}{\Psi(L)} . \tag{1}$$

Voltage:

$$V = B_o \int_a^b U_\theta^\circ(r)\,dr - \frac{I B_o^2}{2\pi} \int_a^b \frac{1}{r\rho U_z \Psi(L)}\,dr . \tag{2}$$

Open-circuit voltage:

$$V_o = B_o \int_a^b U_\theta^\circ(r)\,dr . \tag{3}$$

Short-circuit current:

$$I_{sc} = \frac{V_o}{\frac{B_o^2}{2\pi}\int_a^b \frac{1}{r\rho U_z \Psi(L)}\,dr} . \tag{4}$$

Internal resistance:

$$R_i = \frac{B_o^2}{2\pi}\int_a^b \frac{1}{r\rho U_z \Psi(L)}\,dr . \tag{5}$$

Maximum power:

$$P_{max} = \frac{V_o^2}{\frac{2B_o^2}{\pi}\int_a^b \frac{1}{r\rho U_z \Psi(L)}\,dr} , \tag{6}$$

$$\Psi(z) = 1 - \exp\left(-\frac{\sigma B_o^2 z}{\rho U_z}\right) ,$$

and

$$\sigma' = \frac{\sigma}{1 + (\sigma \beta B_o)^2} .$$

EXPERIMENTAL UNIT

General Description

The experimental unit consists of eight components plus appropriate control instrumentation (fig. 3). The components are as follows: Motor generator, air compressor, air heater, combustor-generator, field magnet, secondary chamber, diverter, and water-spray quencher. The combustor-generator was designed to initially use a gaseous fuel, with possible later modification to permit coal combustion. The combustor, in essence a modified cyclone burner, has a heat release of 1.9×10^6 Btu/(hr)(ft^3) on burning 1,000 ft^3/hr of natural gas; that is, the heat release is equal to 3×10^5 Btu/(hr)(ft^2 of combustor surface). Oxygen-enriched combustion air is preheated to a nominal 1,100° F. Air and fuel pressures are approximately 12 and 8 psig at their respective inlet nozzles, providing an entering velocity of approximately 1,200 ft/sec. The combustion gas moves tangentially and axially along the length of the cyclone burner to a converging-diverging exit nozzle, then through a secondary chamber of somewhat larger internal diameter, through the diverter, and into the water-spray quenching stack.

The field magnet for the generator is an air core solenoid that provides an axial field of 3,000 gauss (0.3 Tesla). Electrical power for the field magnet is furnished by a 70-v, d.c. motor-generator set, rated at 105 kw.

Air heater--Oxygen-enriched combustion air is preheated in a gas-fired heater that employs a helical, pipe-coil, fabricated from 3-in-diam, 310 stainless steel.

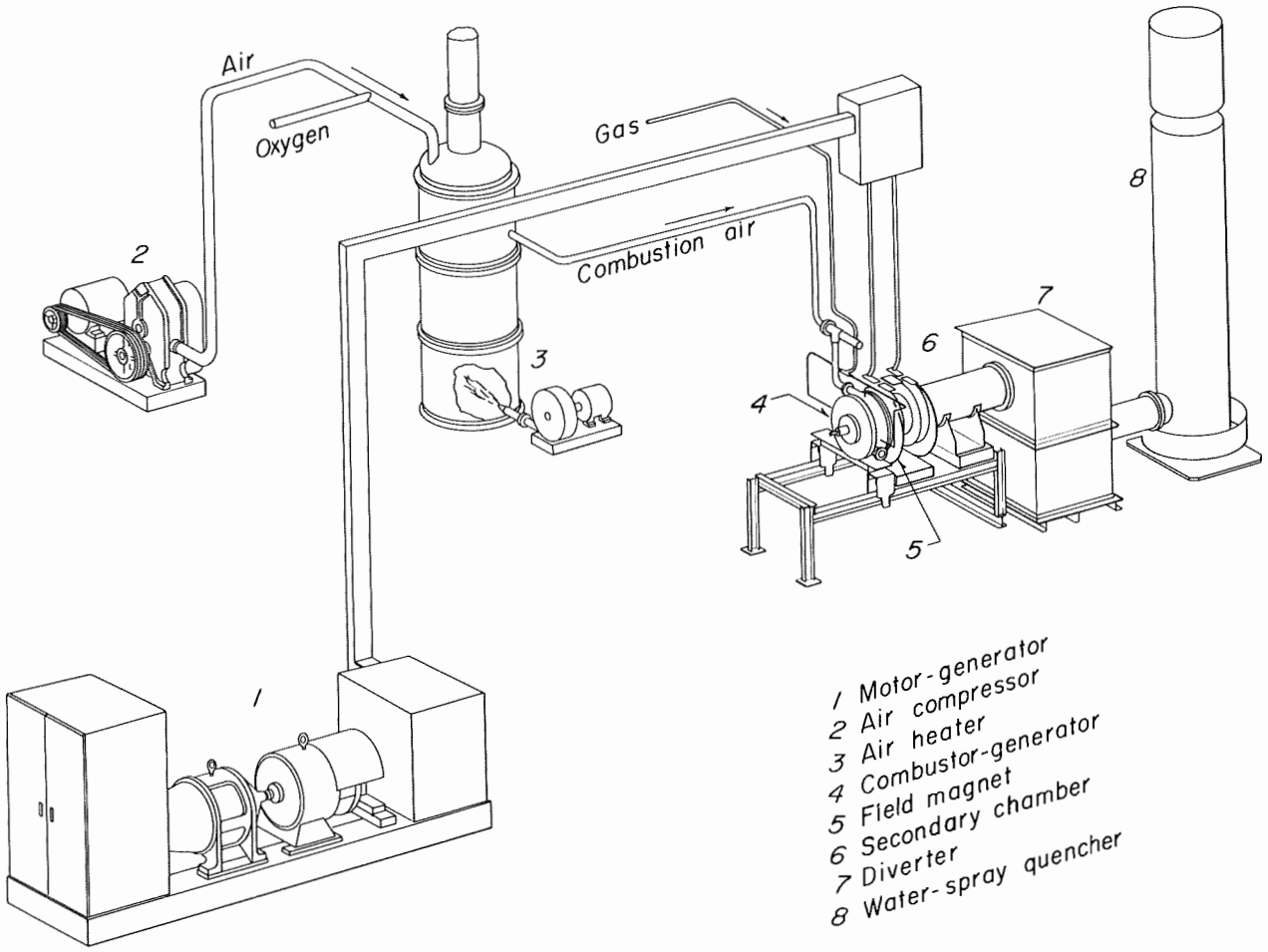

FIGURE 3. - Pictorial View of Vortex MHD Generator.

Combustor-generator--The combustor-generator (fig. 4) is 7½ in ID by 21 in long. The confining walls are composed of refractory rings, 3 in wide with a 2-in wall thickness with mated tongue-and-groove joints. The rings each have four holes, spaced 90° apart penetrating the 2-in-thick walls. These holes permit entry of iridium conductors ("collectors"), which are bonded to the inner surface of the wall and serve to carry currents to the external load circuit. The rings are cast from a 99-percent lime-stabilized zirconia that has a melting point of 4,850° F and a maximum service temperature of 4,200° to 4,600° F. Electrical conductivity of the zirconia refractory rises to a fairly high level at temperatures exceeding 3,600° F, thus permitting it to serve as an electrode. Behind the refractory rings is a lightweight insulating castable of zirconia with a maximum working temperature of 4,000° F. These backup rings are a four-segment, split-ring assembly, 2 in thick. They allow for expansion of the inner hot-face assembly and provide clearance for passage of the electrical conductors. Between the backup rings and the water-cooled jacket there is a ½-in thickness of alumina-silica fiber. This insulation is compressible and therefore does not interfere with the thermal expansion of the rigid refractories.

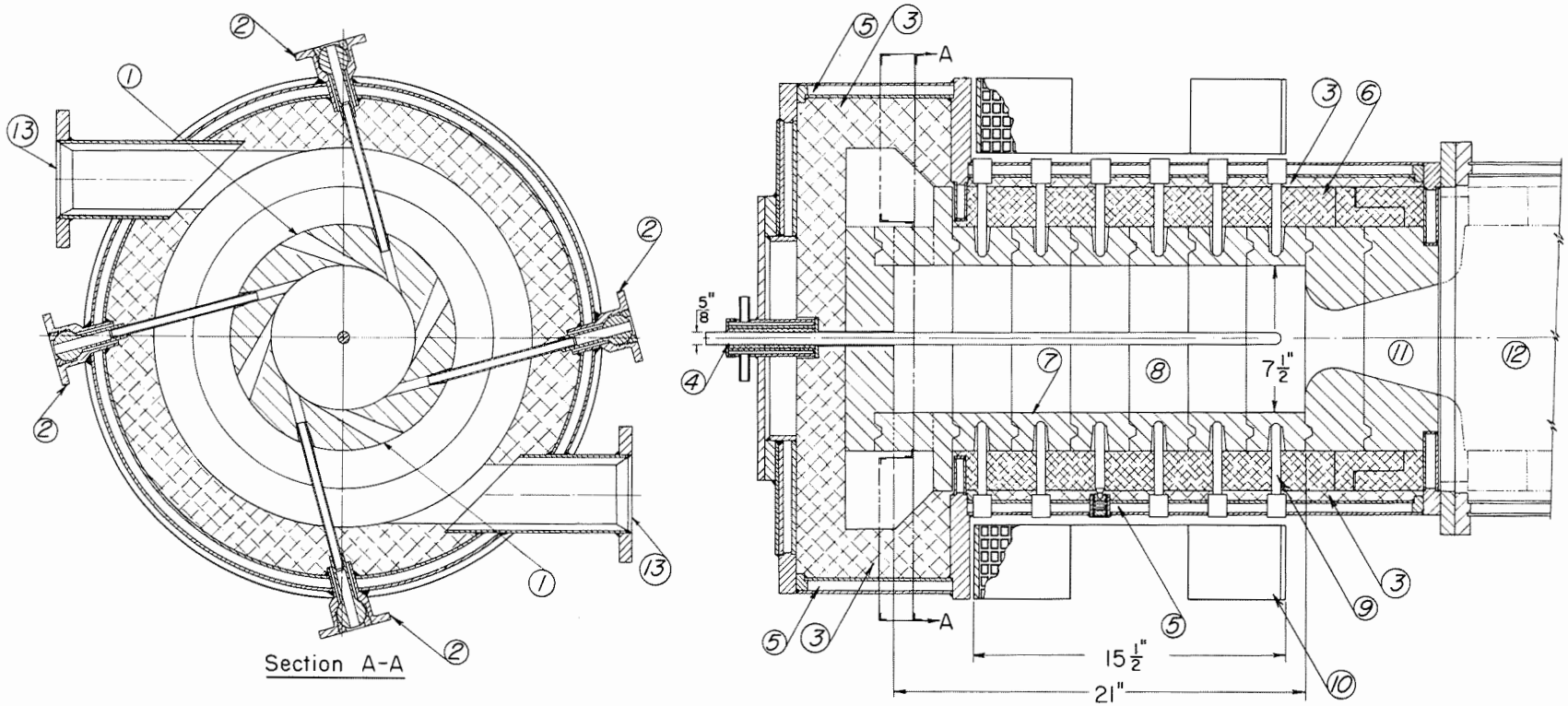

1. Combustion air nozzle
2. Gas nozzle
3. Alumina-silica fiber block
4. Center electrode
5. Water jacket
6. Foamed insulation (zirconia)
7. Refractory electrode (zirconia)
8. Combustion chamber
9. Iridium conductor
10. Magnet
11. Exit nozzle
12. Secondary chamber
13. Combustion air inlet

FIGURE 4. - Vortex MHD Generator.

The water-jacketed vessel totally surrounds the combustor-generator and acts as a gastight enclosure. Internal water passages are provided to direct the cooling water to the more vulnerable locations. Thermocouples at these locations indicate metal surface temperatures. Drain-off from these points is channeled to less critical areas before leaving the vessel. Air enters the cyclone burner tangentially through four sized inlet nozzles which establish the entering velocity. Natural gas enters, also tangentially, through four smaller nozzles sized to provide the same velocity. The fuel gas enters the burner directly, without premixing, to prevent ignition prior to entry.

At the inlet end of the vessel there is an access opening for assembling the combustor-generator's internals. The coverplate for this opening supports a water-cooled holder for the generator's center electrode. The center electrode is a tungsten or iridium rod as determined by combustion conditions. Boron nitride is used as an electrical insulator. Located on this coverplate are ports for observing and probing the plasma to determine temperature, velocity conductivity, etc. Seeding the generator is accomplished by injecting the seeding agents through one of these ports during natural gas combustion.

Field magnet--Magnet windings consist of a two-coil assembly; each coil is composed of 64 turns. The coils are wound from rectangular, copper tubing (1/2-in by 3/4-in by 0.062-in wall) on a stainless steel spool. Each coil has five water inlets and outlets. With the two coils wired in series, a coil current of 1,850 amp provide a magnetic flux intensity of 0.3 Tesla.

Secondary chamber--This unit consists of a cylindrical, water-cooled shell that has a single course of insulating refractory rings, backed up by a ½-in thickness of compressible, alumina-silica-fiber insulation. Wall thickness of the rings is 2 in, and they are cast from the same lightweight zirconia

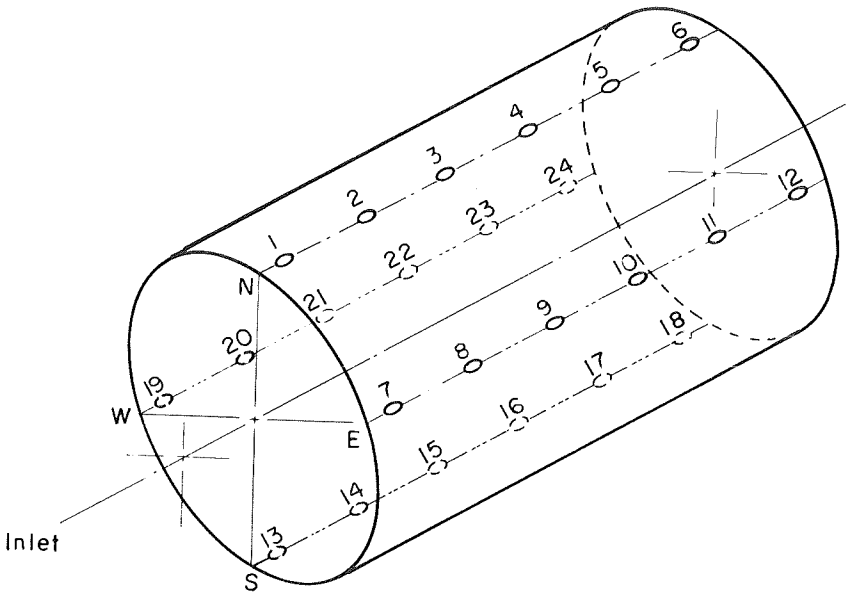

FIGURE 5. - Schematic Arrangement of Collectors, Vortex MHD.

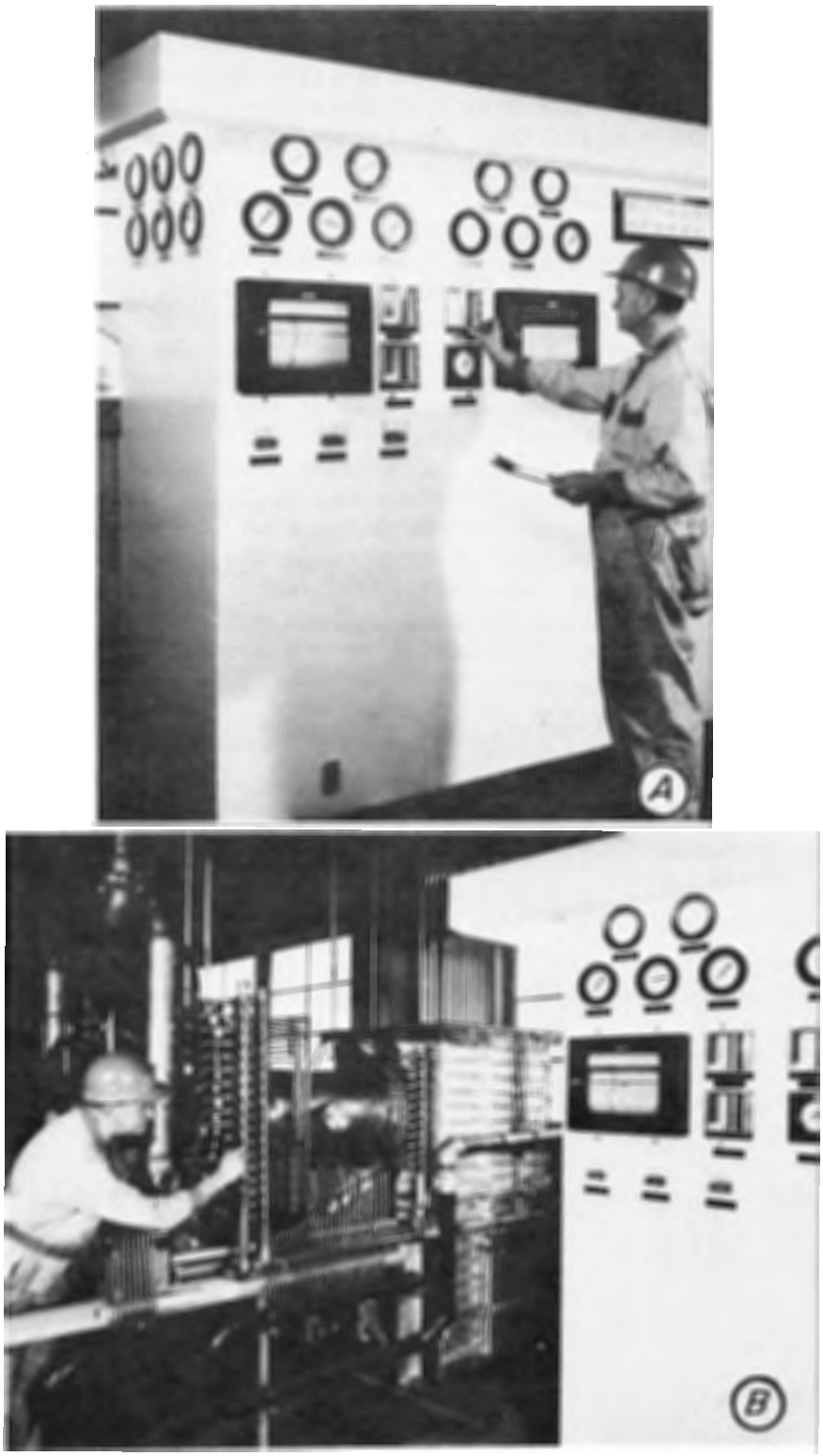

FIGURE 6. - Views of Panelboard and Vortex MHD Generator: *A*, Panelboard; *B*, Vortex.

used in the combustor-generator. The inside diameter of the passage is 11½ in. The chamber is bolted to the exit end of the combustor-generator and attached at the opposite end to the diverter through a bellows expansion joint. There are two 36-in-long ports midway on the chambers and are spaced 180° apart for observation and plasma probing.

Diverter--The diverter is used to change direction of the gas stream, which provides a more desirable elevation for the system to exhaust its hot gases into the quencher. It is a refractory, brick-lined steel box that has two 90° turns to lower the exit elevation without changing the direction of flow. The steel sides, which provide a gastight enclosure, are cooled by copper-tube tracing supplemented by a heat-transfer compound.

Water-Spray Quencher--The flue gas leaving the system flows through a 30-in-diam by 20-ft quench tower, wherein water sprays cool and scrub the gas.

Electrical Collectors--Figure 5

illustrates the arrangement of 24 iridium collectors that carry the current from the six zirconia ring segments that form the chamber wall, through individual wire leads, to a bank of switches at a load box. The leads are then connected to a common load or to individual loads, depending on the test.

OPERATION OF UNIT

A series of electrical generation tests, using natural gas as fuel, took place at the Bruceton facility of the Bureau of Mines in late 1970. A second, similar series took place in early 1971. The purpose of these tests was to provide information to evaluate the capabilities and limitations of the model vortex generator. During the tests, the unit generated small, stable amounts of power at voltages of approximately 2 v. Figures 6a and 6b are photographs of the panelboard and the vortex generator.

Figure 7 shows the heat and material balance around the combustor during a typical test. The "seed" material for these tests was a 3.5-to-1 weight ratio of potassium acetate in water, heated throughout the injection system to 220° F. Fuel and air inlet velocities were ideally 1,200 ft/sec. Seed injection velocity was essentially zero. All combustion parameters were varied somewhat from the values shown in the figure, depending on the requirements of

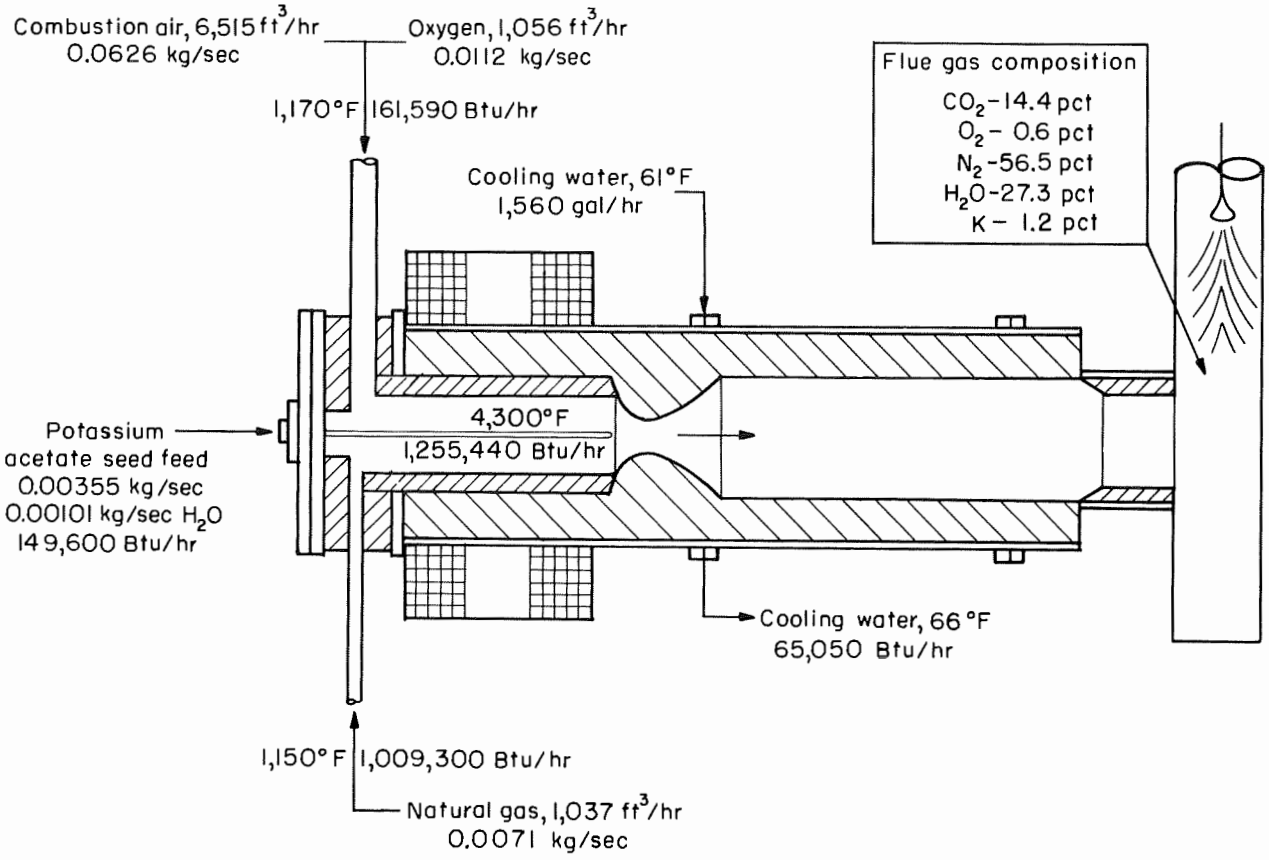

FIGURE 7. - Vortex MHD Gas Combustor, Heat and Material Balance.

the individual tests. Magnet cooling water flow is not included in the diagram because it is not pertinent to heat balance calculations for the generator combustor.

The flame temperature of 4,300° F shown in the figures is a calculated value. Refractory wall temperature at the rear of the chamber, as measured by an electronic 2-color pyrometer, was typically 4,000° to 4,100° F and tended to confirm the calculated flame temperature value. Mixtures were generally close to stoichiometric ratio. Seed levels were in the range 1.0 to 2.0 wt pct in the combustion product gases.

The data of table 1 is typical of results of the "common-load" tests, which were made to measure total power output. In this test, all portions of the generator's outer electrode (all collectors) were connected to a single, adjustable load. The data are plotted in figure 8. If the internally generated voltage V_o and the internal resistance R_i are assumed to remain constant over the range of external resistance R_L, then the equation theoretically describing the functional relationship between V_L and R_L is

$$V_L = V_o - R_i \ (V_L / R_L). \tag{7}$$

TABLE 1. - Electrical output, vortex MHD, single, common load

Load resistance, ohms	V, volts	I, amp	P, watts
2,750	1.80	0.000655	0.00118
737	1.80	.00244	.00440
86.43	1.78	.0206	.0367
8.633	1.73	.200	.347
1.001	1.45	1.45	2.100
.142	.846	5.96	5.040
.0525	.393	7.49	2.942
.0443	.341	7.70	2.625

$V_o = 1.80$ v; $R_i = 0.166$ ohm;

$$P_{max} = \frac{(V_o)^2}{4R_i} = 4.88 \text{ watts}; \ I_{sc} = \frac{V_o}{R_i} = 10.84 \text{ amp}.$$

The value for R_i was determined by a least-squares fit to equation 7; V_o was constrained to 1.80 v. Values of V_o and R_i with derived values of P_{max} and I_{sc} are given at the bottom of table 1. The value of P_{max} is less than that for the observed power at a 0.142-ohm load. This results because P_{max} is calculated from the smooth curve, and the observed power is calculated from the individual observation. Short-circuit current I_{sc}, as obtained from the formula $I_{sc} = V_o / R_i$, is included in the table.

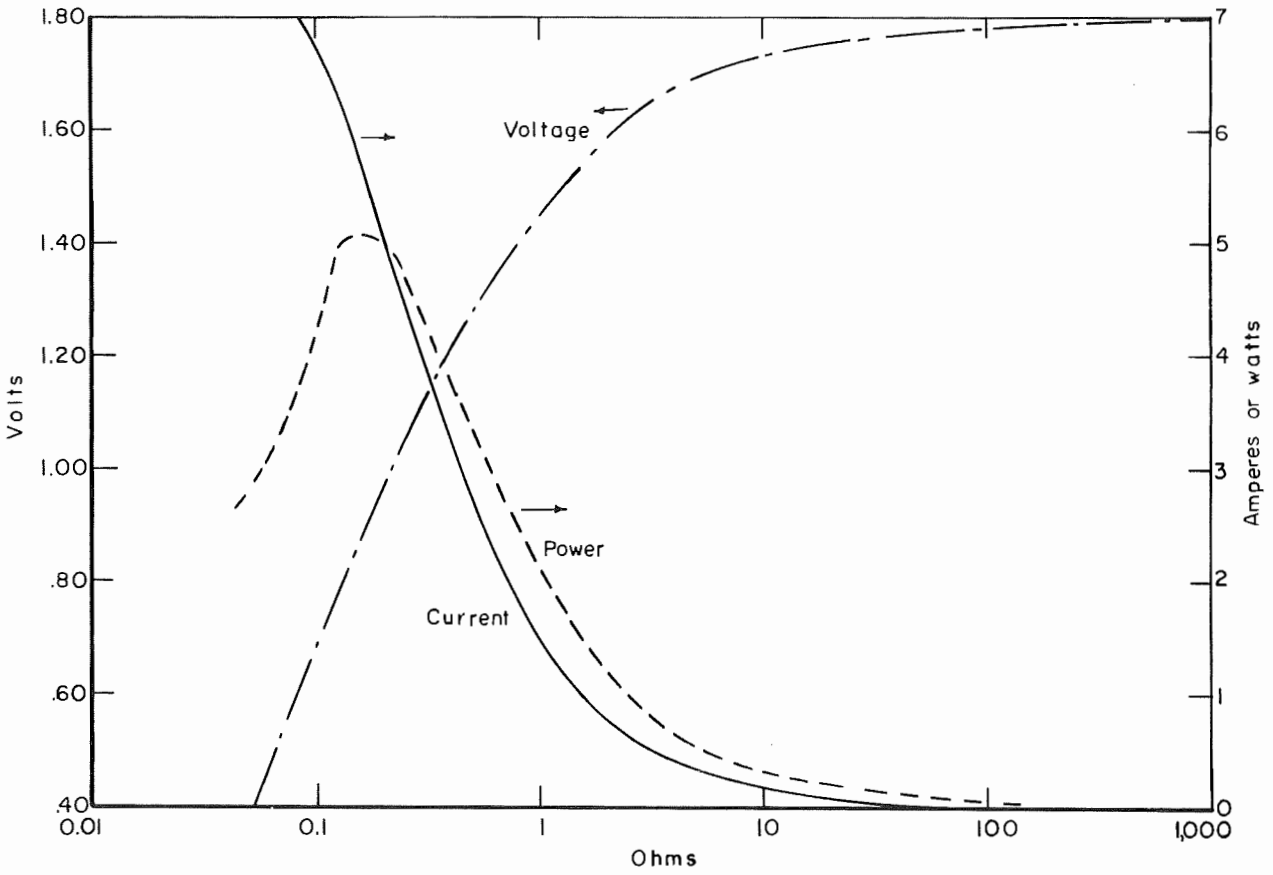

FIGURE 8. - Voltage, Current, Power Versus Load Resistance, Vortex MHD, Common Load Test.

Table 2 shows typical results when the collectors of each of the six-ring segments were connected to six individual loads. These data establish the fact that the rear portion of the generator provided the highest power. Values for V_o and R_i were found by a least-squares fit to equation 7 without constraint on V_o. Figures 9-11 show voltage, current, and power relationships with load resistance for this test. As may be observed from figure 11, in which the individual power curves are plotted, power generated in rings 4-6 was significantly greater than that from rings 1-3. Best-fit constants were calculated for the voltage data to fit equation 7, previously used, and these values are included with table 2. Solving for maximum power values yields the results shown in the table.

Voltage developed across a given load varied from test to test, but did not fluctuate appreciably during the period of each observation. Table 3 lists voltage across a 2,750-ohm load (the highest voltage) for a number of applicable trials, together with information on some of the operating conditions. The data have been analyzed for relationships between voltage and the other variables. Over the small ranges of variables encountered here, no significant correlations occur, although a trend toward increasing voltage as inlet velocity increased is indicated.

TABLE 2. - Electrical output, vortex MHD, segments separately loaded

Segment	Values measured at various load resistance										Values calculated from equation 7			
	0.380 ohm			0.687 ohm			0.968 ohm			100 ohms, V, volts				
	V, volts	I, amp	P, watts	V, volts	I, amp	P, watts	V, volts	I, amp	P, watts		V_o, volts	R_i, ohms	P_{max} watts	I_{sc}, amp
1	0.400	1.053	0.420	0.535	0.779	0.417	0.700	0.723	0.506	0.965	1.207	0.777	0.469	1.553
2	.470	1.237	.583	.635	.924	.587	.790	.816	.645	1.16	1.332	.706	.628	1.887
3	.460	1.211	.557	.625	.910	.569	.755	.780	.589	1.14	1.252	.661	.593	1.894
4	.580	1.526	.887	.770	1.121	.862	.880	.909	.800	1.40	1.316	.483	.896	2.725
5	.620	1.632	1.011	.825	1.201	.990	.950	.981	.932	1.49	1.437	.503	1.026	2.857
6	.627	1.650	1.035	.831	1.210	1.006	.953	.985	.939	1.49	1.428	.487	1.047	2.932
Total or equiv.[1]	.541	8.309	4.493	.721	6.145	4.431	.849	5.194	4.411	1.27(avg)	1.346	.097	4.663	13.88

[1] Equivalent voltages shown are those that would appear across a single load dissipating the indicated power at the associated current.

TABLE 3. - Voltage at 2,750-ohm load, various runs[1]

Run	Load voltage, v	Temp, ° F	Gas comp.[2]	Inlet velocity, ft/sec	Seed level in gases		Run	Load voltage, v	Temp, ° F	Gas comp.[2]	Inlet velocity, ft/sec	Seed level in gases	
					Wt pct	Mole pct						Wt pct	Mole pct
70/1	1.45	3,900	Fuel...	1,206	1.22	0.86	71/2	1.65	4,020	Oxygen.	1,409	1.54	1.10
70/2	[3]1.43	4,020	..do...	1,206	1.22	.86	71/4	2.14(calc.)	4,010	Fuel...	1,375	1.69	1.20
70/2	[4]1.41	4,010	..do...	1,206	1.22	.86	71/5	[3]2.05	4,015	..do...	1,375	1.70	1.21
70/3	[3]1.42	3,970	Oxygen.	1,205	2.37	1.67	71/5	[4]1.82	4,020	..do...	1,375	1.70	1.21
70/3	[4]1.42	3,960	Fuel...	1,205	2.37	1.67	71/6	[2]2.02	4,035	..do...	1,375	1.70	1.21
70/4	[3]1.44	3,960	Stoich.	1,205	2.37	1.67	71/6	[4]2.05	4,035	..do...	1,375	1.70	1.21
70/4	[4]1.40	3,980	Fuel...	1,205	2.37	1.67	71/7	2.15(calc.)	4,115	..do...	1,375	1.70	1.21
70/5	1.43	3,970	Oxygen.	1,447	1.38	.98	71/8	2.08	4,115	..do...	1,624	1.48	1.09
							71/9	1.35(calc.)	4,115	..do...	1,624	1.48	1.09
							71/10	[3]1.68	4,115	..do...	1,624	1.48	1.09
							71/10	[4]1.80	4,115	..do...	1,624	1.48	1.09

[1] Tests listed are those applicable to voltage comparison.
[2] Effluent condition: excess fuel, excess oxygen, or stoichiometric mixture.
[3] Beginning of test.
[4] End of test.

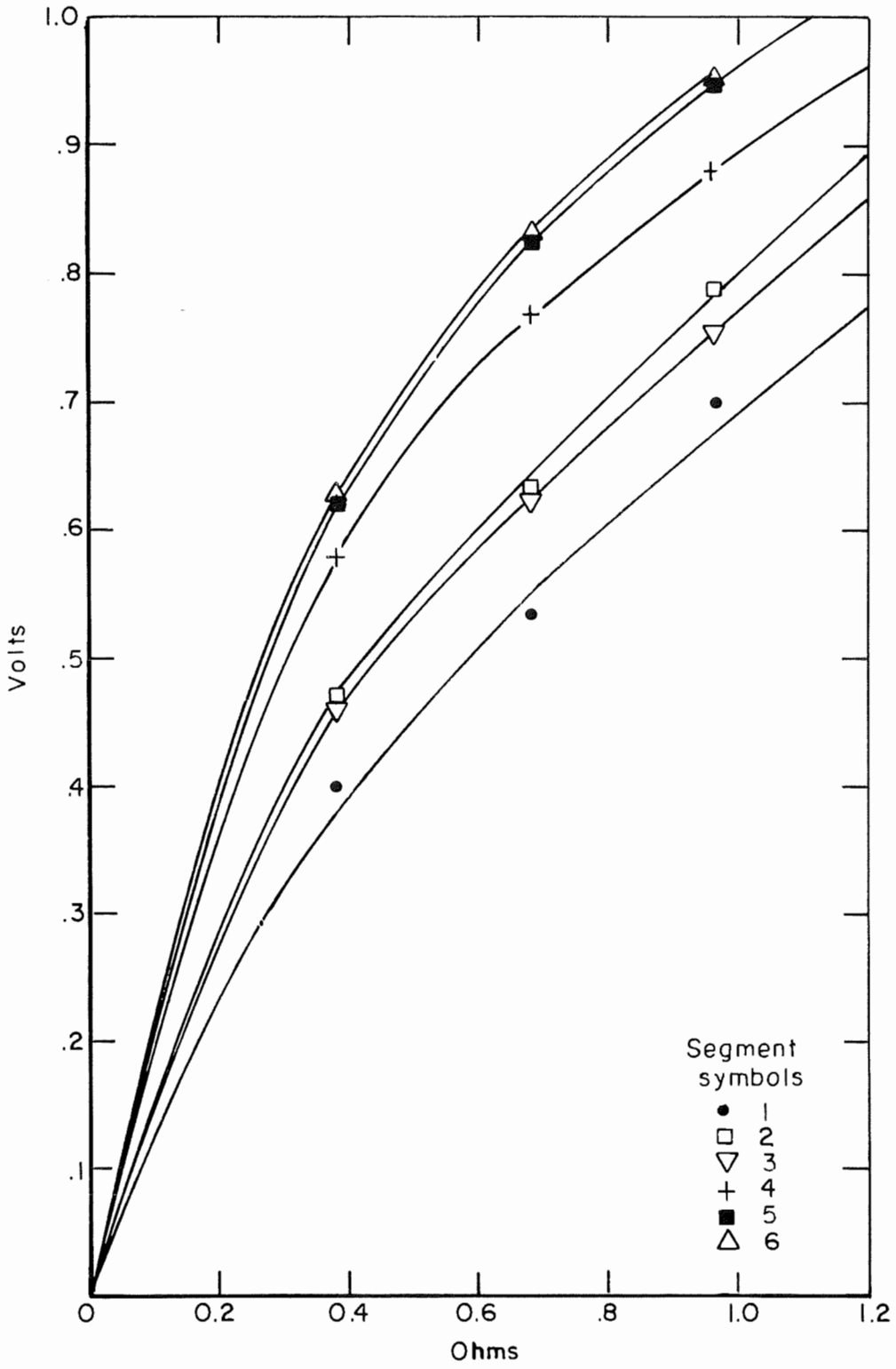

FIGURE 9. - Load Voltage Versus Load Resistance, Vortex MHD, With Segments Separately Loaded.

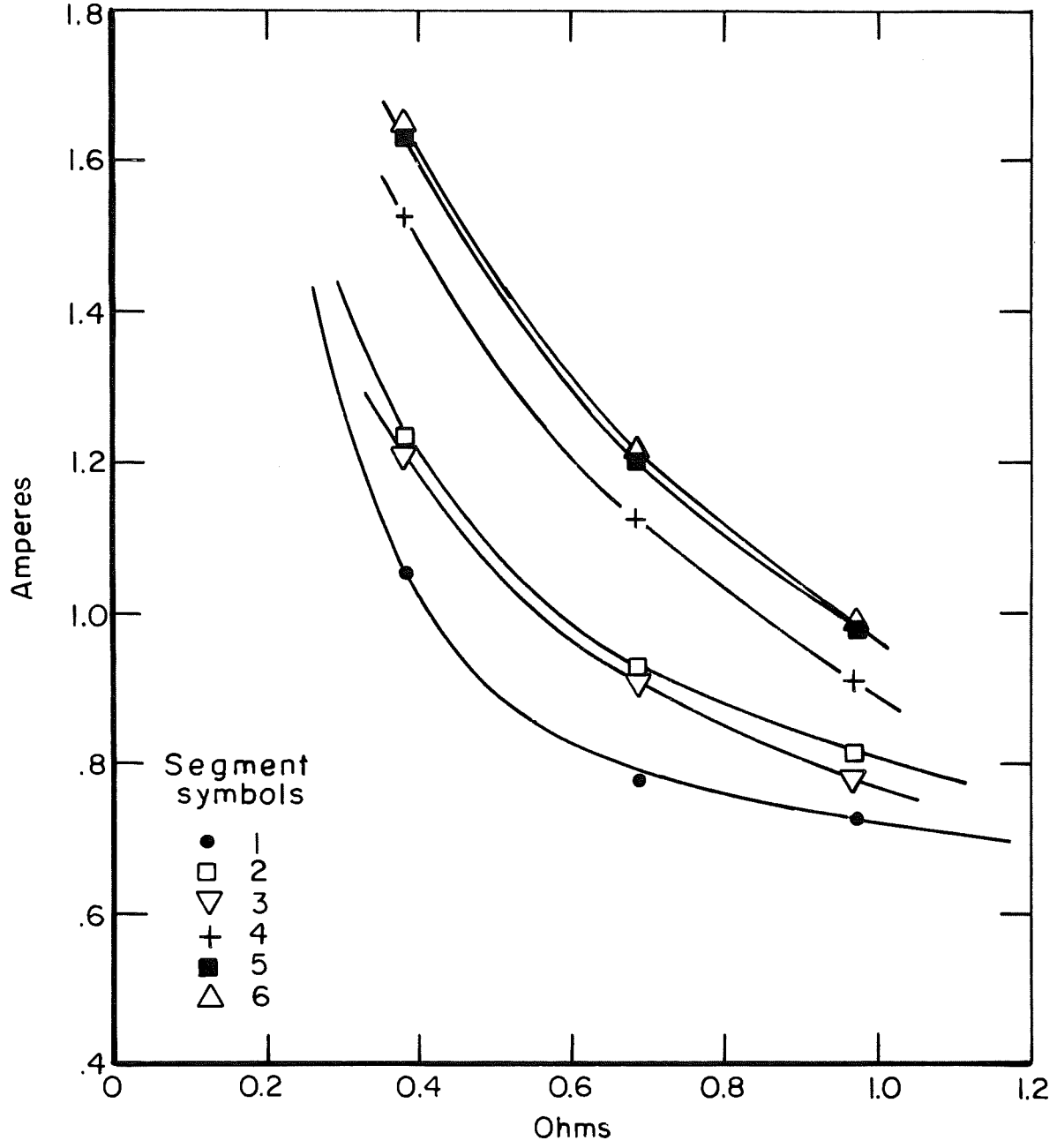

FIGURE 10. - Load Current Versus Load Resistance, Vortex MHD, With Segments Separately Loaded.

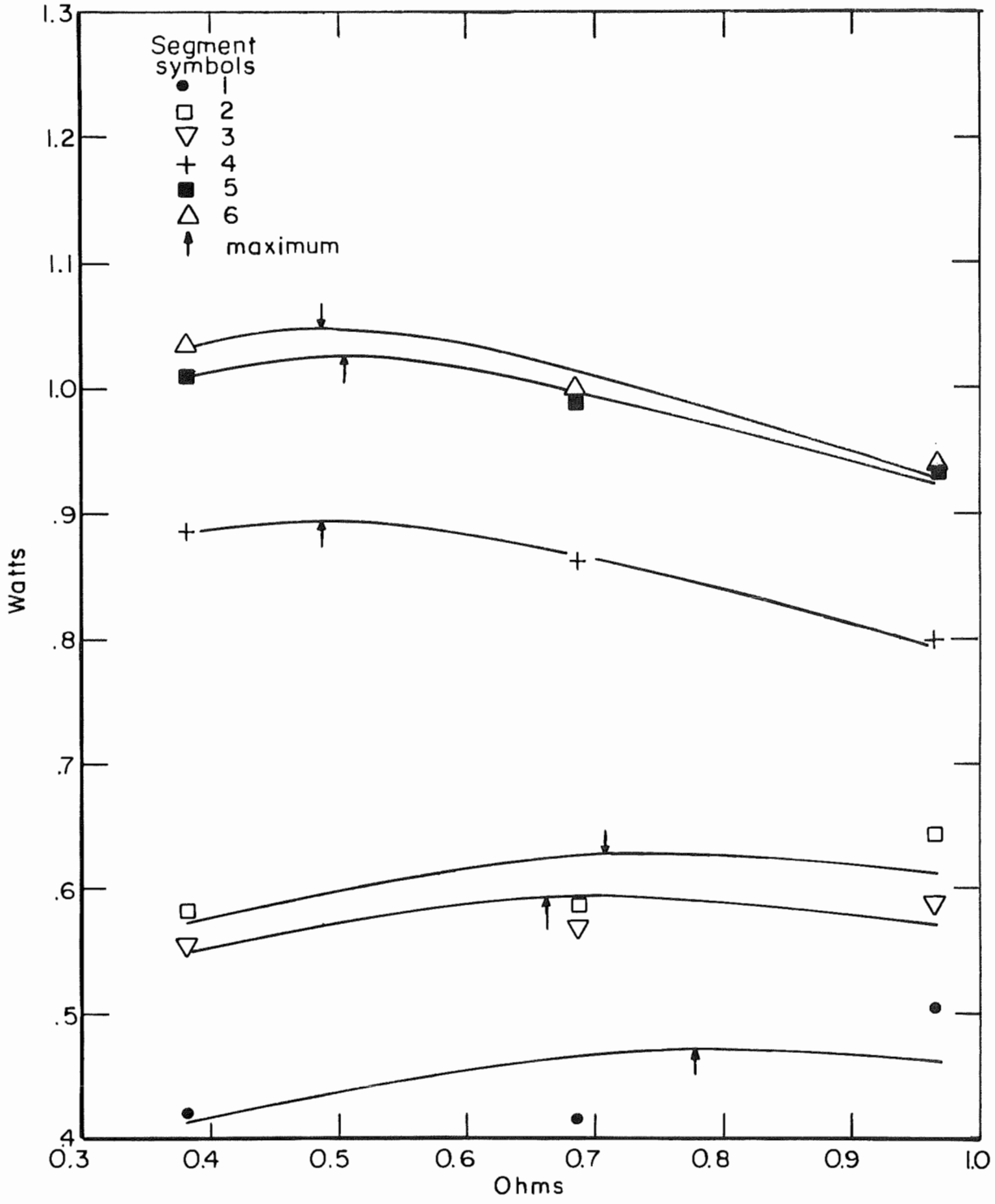

FIGURE 11. - Power to Load Versus Load Resistance, Vortex MHD, With Segments Separately Loaded.

L-12445

With regard to vortex flow, no velocity measurements were made at the operating temperature. Measurements were taken at room temperature, yielding the data of tables 4 and 5. Adjustment to the 1,200 ft/sec calculated operational inlet velocity results in the curve shown in figure 12; and normalization and averaging yields the curve shown in figure 13.

TABLE 4. - Tangential velocity variation with radius (no magnetic field)

Radius, in	V_θ (ft/sec) at various z (in)				
	0	1	2	4	6
0.5	68	-	17	0	0
1.0	68	-	33	0	77
1.5	113	192	60	60	82
2.0	180	192	103	84	95
2.5	225	192	111	91	118
3.0	274	281	226	145	146
3.5	615	481	402	263	229
3.62	[1]715	[1]543	[1]403	[1]303	[1]270
3.75	[2]0	[2]0	[2]0	[2]0	[2]0

[1]Maximum values.
[2]Theoretical values.

TABLE 5. - Additional maximum values versus z

Tangential velocity versus z		Value near wall	
z, in	V_θ, ft/sec	z, in	V_θ, ft/sec
3	337	9	236
5	280	10	228
7	250	11	222
8	244	12	213

Collector and zirconia wall resistances were monitored between tests by imposing a constant current and recording the resulting voltages. The values at operational temperature did not change significantly, which indicates that the iridium collectors did not deteriorate throughout the tests. Average collector resistance at full temperature was 0.239 ohm, and average zirconia resistance from one set of collectors to the next was 0.064 ohm.

Center electrodes made of tungsten provided 15 to 20 min of operation, under stoichiometric or slightly reducing conditions. A plasma-sprayed zirconia coating 10 mils thick increased electrode life to approximately 30 min under these conditions. Center electrodes made of thin-wall iridium tubing, though fragile and therefore easily damaged by the turbulent gases, were long lived with all mixtures tested, including 2 pct excess oxygen in the effluent.

The physical effect of the natural gas tests on the zirconia shell was not severe. During initial operation, probably to a large extent during the cooling period, z-direction cracks developed in the zirconia rings. These

cracks did not broaden significantly in subsequent trials, and apparently their contact resistance at operating temperature (with the material expanded and therefore in intimate contact) was not sufficient to adversely affect the conductivity of the rings.

Erosion of boron nitride nozzle liners was significantly rapid, which indicated unsuitability of this material for the purpose in long-term equipment. Its use as an insulator in the water-cooled holder of the center electrode proved satisfactory. Slip-cast zirconia tubes used as nozzle liners also had short life: cracks developed owing to thermal shock. Nozzle holes integrally cast into the zirconia ring eroded slowly, notably at the exit edges of the holes, the perimeter increasing approximately 50 pct during 1,000 hr of operation.

DISCUSSION OF RESULTS

In analyzing the electrical performance of the vortex generator, a key concern is the magnitude and shape of the function $U_\theta^\circ(r)$, the tangential velocity distribution that exists when no magnetic interaction is present. The generated voltage, as described by equation 3, is linearly proportional to the integral of the function. The power delivered to the load is

$$P = \frac{R_L B_o^2}{(R_i + R_L)^2} \left[\int_a^b U_\theta^\circ(r)\,dr \right]^2 .$$

Thus, power is proportional to the square of the integral.

Implicit in the theoretical treatment included as an appendix is the assumption that the tangential velocity, except for magnetic interaction effects, is independent of z, the distance along the axis. Figure 12 contradicts this assumption, showing maximum velocity versus z as a hyperbolically decreasing function. Presumably this decrease is due to wall drag and the failure of assumption a to hole. With the small ratio of diameter to depth found in this unit, there is opportunity for wall friction to become important. The decrease of tangential velocity ratio with decreasing radius (fig. 13) may be a further result of the decrease in absolute value with increasing z. For the electrical power output of the vortex generator to be of useful magnitude, the curve in figure 1 should decidedly increase with decreasing radius. That higher output is possible is shown by previous investigators utilizing vortex chambers with large ratios of diameter to depth.[4]

The effect of the magnetic field in retarding the rotational flow of free electrons in the gas stream cannot be construed as a factor that could moderate the decline of the function: maximum velocity versus z. Since this is true, a calculation of theoretical output may be made by neglecting the magnetic field's influence and then considering each of the six segments of the generator separately, using for each segment the average at beginning and end

[4]Thompson Ramo Wooldridge Inc. Research and Development on a Vortex MHD Power Generator, Final Report. Contract No. NASS-703 NASA, December 1961, 146 pp.

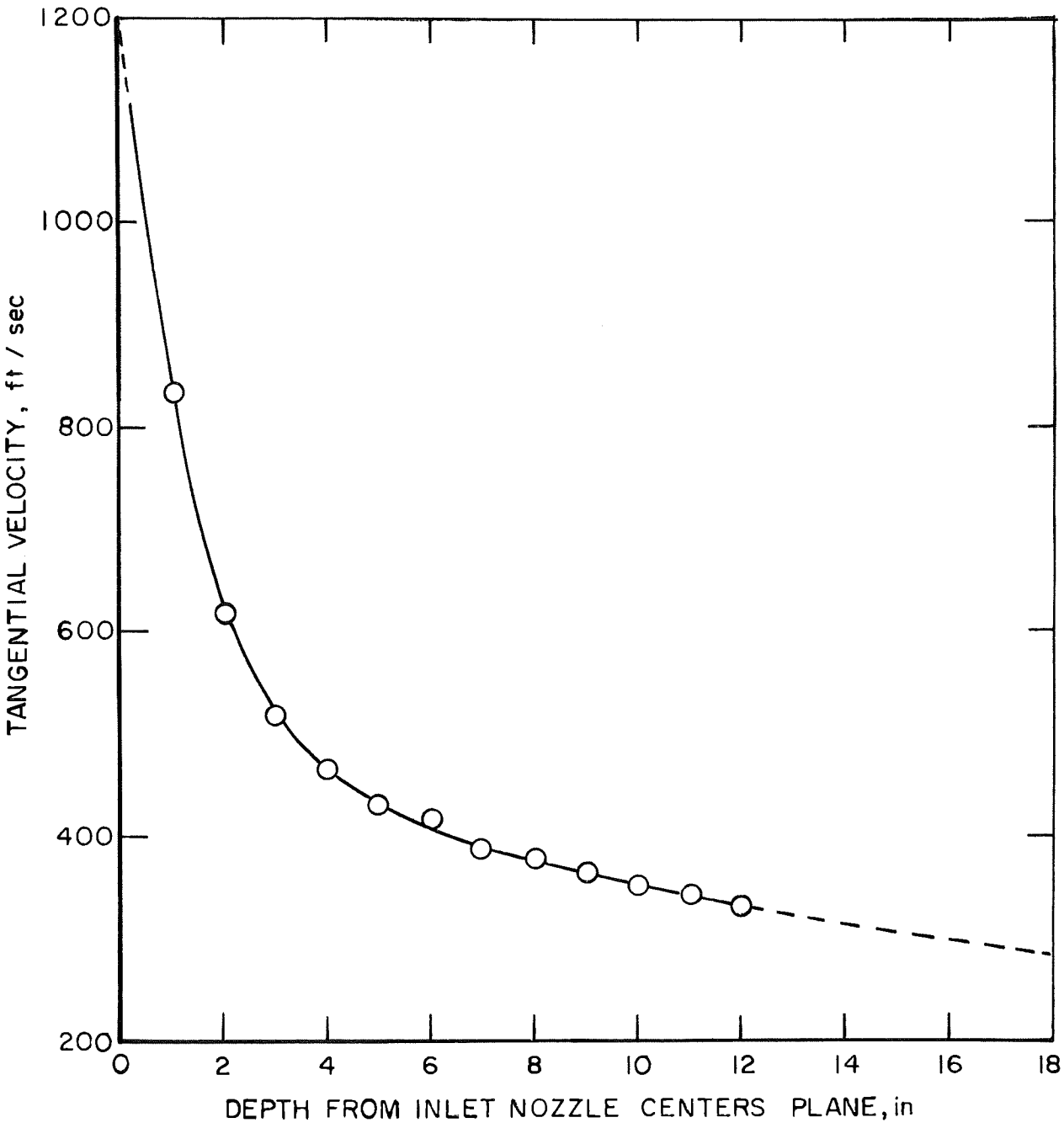

FIGURE 12. - Maximum Tangential Velocity Versus Depth From Inlet Centers Plane (Close to Wall of Vortex MHD).

of the segment of the maximums taken from figure 12, and utilizing the resulting figure 13 integral in the output equations. When this is done and the results are compared with table 2 entries, the total current and power values are found to be within about 15 pct of the measured values, falling below the measured output. This indicates that the power obtained during the trial was all that could be expected, considering the available tangential velocities.

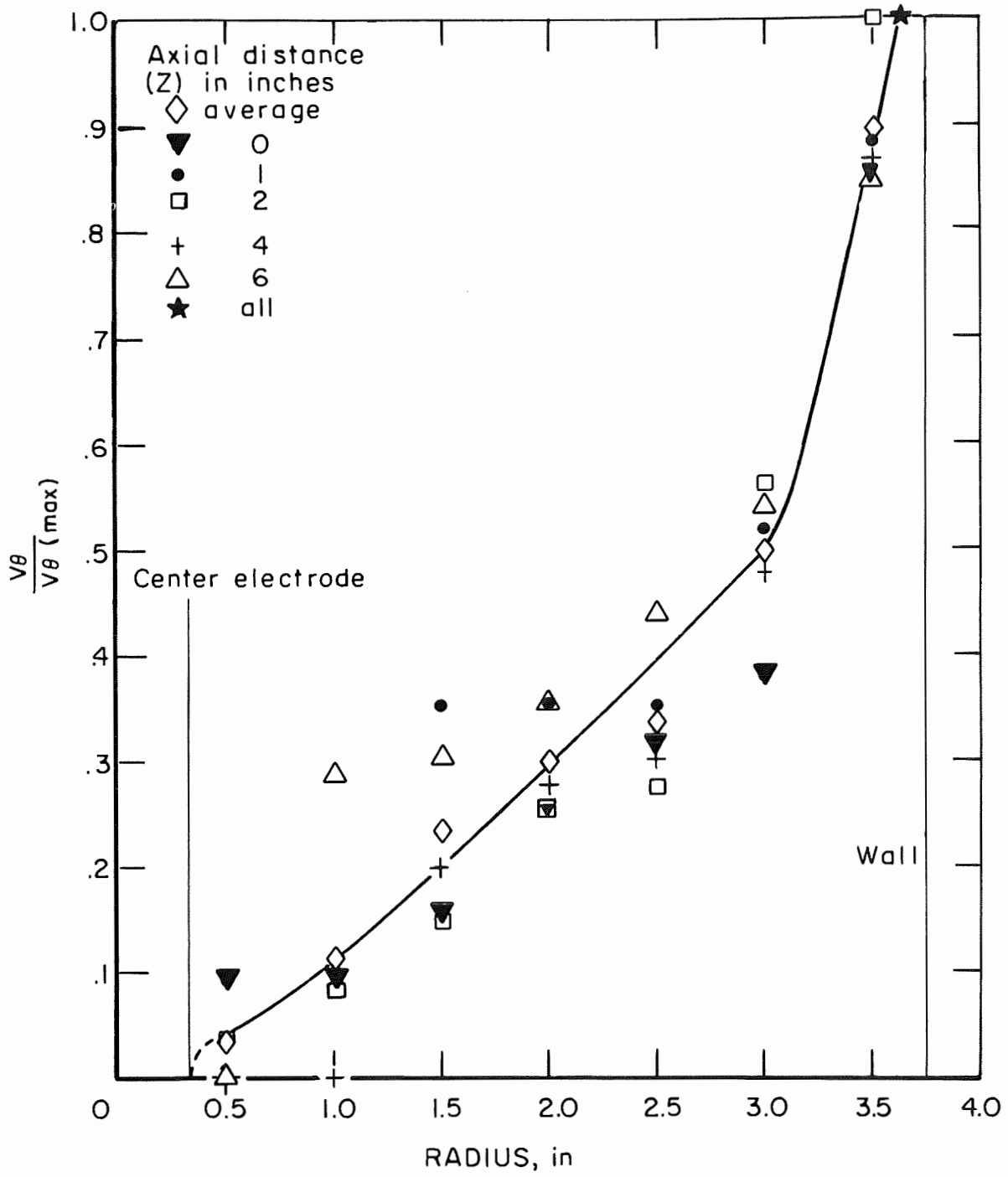

FIGURE 13. - Ratio: $\frac{\text{Tangential Velocity}}{\text{Maximum Tangential Velocity}}$ Versus Radius, Vortex MHD.

The calculated output distribution among the segments is opposite to that of table 2; that is, the smaller contribution of the calculated output is from the rear segments, whereas in actuality these are the most effective generating portions. An explanation for the disparity may be that since axial

velocity, which is due to the expansion flow as combustion occurs, is not negligible compared with the excessively reduced tangential velocity, the flame is quickly swept to the rear of the chamber before the seed has been fully converted to the form of free ions and electrons. Thus the electrical conductivity of the gas in the front portion of the chamber is low, and output voltage for a given current is lower for the front segments than for those at the rear.

With regard to the aforementioned observations, it is desirable to remark that assumptions f and g are not rendered invalid for the generator as originally conceived, just because a potential difference with z can be found in the present model. For purposes of testing, the collectors of this unit were individually connected to the load box through leads which have resistances which are not negligible. In the original design, all collectors are commonly grounded to the outer shell; thus assumption f validity is a forced condition, and assumption g follows. It should be further noted that current flows of the magnitude originally envisaged would tend to cause greater heating of the current paths in the zirconia, thereby increasing their conductivity and further contributing to the validity of assumption f by increasing the overall conductivity of the zirconia shell.

CONCLUSIONS

Power generation was lower than calculated because theoretical plasma velocities were not achieved. In a practical vortex MHD generator, tangential velocity must be high, and should increase with decreasing radius, while remaining substantially independent of axial distance z. Axial velocity should be small compared with tangential velocity. A unit with an effectively large ratio of diameter to depth, in which some combustion occurs before the nozzles, can accomplish these requirements. For an effectively large ratio, given the restriction that depth cannot be reduced at will, z-directional slots may be used in place of the single ring of nozzles used in the present model. A diameter that is actually large is still advantageous because of low relative wall drag and because, if water-cooled structures are included in the wall, the heat loss due to these structures is less important for a large-diameter unit.

Although the electrical output of this small-scale vortex MHD generator was limited, the natural-gas-fueled tests provided information pertinent in any study to determine design requirements for a practical vortex MHD generator.

In particular, several materials problems of the insulating and electrode portion of the channel were studied experimentally. Generally, one can conclude that given an inlet velocity from the swirl nozzles, power can be extracted nearly equal to that predicted theoretically. However, in this experiment combustion took place entirely within the vortex chamber, and high velocities were not obtained. If a portion of the combustion were to take place in or before the nozzle, then the swirl velocity could be increased to a high enough value to give significant power output levels.

BIBLIOGRAPHY

1. Coerdt, R. J., W. C. Davis, R. T. Craig, and J. E. McCune. A Vortex MHD Power Generator. Ch. in Energy Conversion for Space Power, ed. by N. W. Snyder, Academic Press, New York, 1961, pp. 695-710.

2. Elco, R. A., W. F. Hughes, and F. J. Young. Theoretical Analysis of the Radial Field Vortex Magnetogasdynamic Generator. J. Appl. Math. and Phys., v. 13, 1962, pp. 1-13.

3. Hughes, W. F., and F. J. Young. The Electromagnetodynamics of Fluids. Wiley & Sons, Inc., New York, 1966, 648 pp.

4. McCune, J. E., and C. Donaldson. On the Magnetogasdynamics of Compressible Vortices. Ch. in Energy Conversion for Space Power, ed. by N. W. Snyder, Academic Press, New York, 1961, pp. 715-741.

5. Sutton, G. W., and A. Sherman. Engineering Magnetohydrodynamics. McGraw-Hill Book Co., Inc., New York, 1965, 548 pp.

6. Thompson Ramo Wooldridge Inc. Research on the Vortex MHD Power Generator, Final Report. Contract NAS 3-2526 NASA, July 1963, 154 pp.

APPENDIX A.--DERIVATION OF VORTEX MHD GENERATOR EQUATIONS

The following derivations originate in a report by Thalimer, Kurtzrock, Simons, Bienstock, and Hughes.[1] Certain nomenclature changes have been made in the appendix to avoid confusion in applying the development to the present report.

The gas flow in the generator is idealized to the extent given by the following assumptions:

(a) The gas is inviscid, and boundary layer effects are confined to a thin layer along the electrode surfaces. Effects of secondary flow due to viscosity are neglected.

(b) The radial velocity is everywhere zero. In actuality, the injected gas has an initial small radial velocity component. However, we are assuming that complete diffusion to the center electrode has taken place before the interaction region.

(c) The flow is axially symmetric; that is, all quantities are independent of θ.

(d) The magnetic Reynolds number is small so that the applied magnetic field, B_θ, is essentially unchanged, and induced fields can be neglected.

(e) The flow is in steady state.

The equations that describe the electrical and mechanical behavior of the gas follow.

The continuity equation is

$$\nabla\cdot(\rho\vec{U}) = 0, \tag{1A}$$

where ρ is the mass density of the gas and $\vec{U}$ is the velocity.

The equation of motion is

$$\rho\,\frac{D\vec{U}}{Dt} = \rho\left[\frac{\partial\vec{U}}{\partial t} + (\vec{U}\cdot\nabla)\vec{U}\right] = -\nabla P + \vec{J}\times\vec{B}, \tag{2A}$$

where P is the pressure, $\vec{J}$ is the current density, $\vec{B}$ is the magnetic field, and $\frac{D}{Dt}$ is the material derivative.

---

[1] Thalimer, J. R., R. C. Kurtzrock, W. H. Simons, D. Bienstock, and W. F. Hughes. Design of an Open-Cycle, Vortex MHD Generator. Ch. in Electricity From MHD, 1968. Internat. Atomic Energy Agency, Vienna, 1968, pp. 2601-2612.

Ohm's law is

$$\vec{J} = \sigma\ (\vec{E} + \vec{U} \times \vec{B} - \beta\vec{J} \times \vec{B}), \tag{3A}$$

where σ is the scalar conductivity, $\vec{E}$ is the electric field, $\beta = 1/e\ N_e$, e is the electronic charge, and N_e is the electron density. Currents due to gradients in the electron partial pressure and ion slip terms are neglected. From Maxwell's equations, we will use

$$\nabla\cdot\vec{J} = 0 \tag{4A}$$

and

$$\nabla\times\vec{E} = 0. \tag{5A}$$

By appending two additional assumptions to our list, we can solve the above system of equations. The first of these assumptions is as follows:

(f) The conductivity of the electrodes is much greater than that of the gas, so that the axial component of the electric field in the electrodes is zero.

The second additional assumption is motivated by the observation that the terminal voltage, given by

$$V = -\int_a^b E_r\ d\ r$$

is independent of z since the electrodes are continuous. Therefore, we will assume

(g) E_r is independent of z; that is, $E_r = E_r(r)$.

From equation 5A it follows immediate that $E_\theta = 0$.

In view of assumption d, we can use assumption b and the above equation to write the components of J as

$$J_r = \frac{\sigma}{1 + (\sigma\beta B_o)^2}\ (E_r + U_\theta B_o),$$

$$J_\theta = \sigma\beta B_o\ J_r,$$

and

$$J_z = \sigma E_z.$$

Since by g, E_r is not a function of z, it follows from equation 5A that $\frac{\partial E_z}{\partial r} = 0$, and hence E_z depends only on z. But from f we have for any z, that $E_z = 0$ at $r = b$, and thus this equality holds everywhere.

It is worth noting that if J_r is written as

$$J_r = \sigma'\ (E_r + U_\theta B_o), \tag{6A}$$

where $\sigma' = \frac{\sigma}{1+(\sigma\beta B_o)^2}$, then all the results involving J_r can be interpreted as including or not including Hall effects, depending upon whether or not β is considered in the analysis.

The θ-component of equation 2A is

$$\rho U_z \frac{\partial U_\theta}{\partial z} = -J_r B_o .$$

Combining this with equation 6A, we obtain the equation

$$\frac{\partial U_\theta}{\partial z} + \frac{\sigma' B_o^2 U_\theta}{\rho U_z} + \frac{\sigma' B_o E_r}{\rho U_z} = 0 \tag{7A}$$

for $U_\theta = U_\theta(r,z)$. This equation becomes tractable upon observing that, since equation 1A is reduced to

$$\frac{\partial(\rho U_z)}{\partial z} = 0,$$

ρU_z is a function of r only.

If we denote the inlet tangential velocity profile $U_\theta(r,0)$ by $U_\theta^\circ(r)$, it can be readily verified that

$$U_\theta(r,z) = U_\theta^\circ(r) \exp\left(-\frac{\sigma' B_o^2 z}{\rho U_z}\right) - \frac{E_r}{B_o}\Psi(z), \tag{8A}$$

where $$\Psi(z) = 1 - \exp\left(-\frac{\sigma' B_o^2 z}{\rho U_z}\right),$$

is a solution of equation 7A satisfying the boundary condition

$$U_\theta(r,0) = U_\theta^\circ(r). \tag{9A}$$

To show that equation 8A is the unique solution, let $W(r,z) = U_\theta(r,z) - f_\theta(r,z)$ where $f_\theta(r,z)$ is any function satisfying equation 7A and such that $f_\theta(r,0) = U_\theta^\circ(r)$. Then $W(r,0) = 0$ and

$$\frac{\partial W}{\partial z} + \frac{\sigma' B_o^2 W}{\rho U_z} = 0. \tag{10A}$$

Whenever $W(r,z) \neq 0$, equation 10A can be written as

$$\frac{\partial \ln W}{\partial z} = -\frac{\sigma' B_o^2}{\rho U_z},$$

and thus, except when $W(r,z) = 0$,

$$W(r,z) = Q(r) \exp\left(-\frac{\sigma' B_o^2 z}{\rho U_z}\right), \tag{11A}$$

where Q is a function of r yet to be determined. However, since $W(r,z)$ is continuous, equation 11A holds for all values of r and z. In particular,

$$0 = W(r,0) = Q(r)$$

and it follows that $W(r,z) = 0$. Therefore, $U_\theta(r,z) = f_\theta(r,z)$, which proves that equation 8A is the unique solution of equation 7A satisfying equation 9A.

By definition, $I = \int_A \vec{J}\cdot d\vec{A}$, so with r = b we have $I = 2\pi b \int_0^L J_r(b,z)\,dz$. But from equation 4A, $J_r = J_r(r,z) = \frac{f(z)}{r}$, where f is a function of z only. Therefore

$$I = 2\pi r \int_0^L J_r\, dz. \tag{12A}$$

If equation 8A is used in equation 6A, the integration of J_r in equation 12A can be explicitly performed. The resulting equation, when solved for E_r, yields

$$E_r = B_o\left[\frac{I B_o}{2\pi r \rho U_z \Psi(L)} - U_\theta^\circ(r)\right]. \tag{13A}$$

In final summary (with equation numbering as it appears in the present report), equation 1 is obtained by substituting equation 13A into equation 8A. The terminal voltage, V, is given by

$$V = \int_a^b E_r\, dr,$$

and by using equation 13A, can be written as equation 2. The open circuit voltage, V_o, can be calculated by setting I = 0 in equation 2. The result is equation 3.

The short circuit current, as given by equation 4, is obtained by setting V = 0 in equation 2 and solving for I.

Equation 5 is the internal resistance of the generator given by $R_i = V_o / I_{sc}$.

The maximum power output, P_{max}, as given in equation 6 is $V_o I_{sc}/4$.

The principal results of the generator analysis are therefore:

$$U_\theta = U_\theta^\circ(r) - \frac{I B_o}{2\pi r \rho U_z} \cdot \frac{\Psi(z)}{\Psi(L)} ; \tag{1}$$

$$V = B_o \int_a^b U_\theta^\circ(r)\,dr - \frac{I B_o^2}{2\pi} \int_a^b \frac{1}{r \rho U_z \Psi(L)}\,dr; \tag{2}$$

$$V_o = B_o \int_a^b U_\theta^\circ(r)\,dr; \tag{3}$$

$$I_{sc} = \frac{V_o}{\frac{B_o^2}{2\pi} \int_a^b \frac{1}{r \rho U_z \Psi(L)}\,dr} ; \tag{4}$$

$$R_i = \frac{B_o^2}{2\pi} \int_a^b \frac{1}{r \rho U_z \Psi(L)}\,dr; \tag{5}$$

$$P_{max} = \frac{V_o^2}{\frac{2B_o^2}{\pi} \int_a^b \frac{1}{r \rho U_z \Psi(L)}\,dr} ; \tag{6}$$

where I is the total current, $U_\theta^\circ(r)$ is the inlet tangential velocity profile,

$$\Psi(z) = 1 - \exp\left(-\frac{\sigma' B_o^2 z}{\rho U_z}\right),$$

$$\sigma' = \frac{\sigma}{1 + (\sigma \beta B_o)^2},$$

V is the terminal voltage, V_o is the open circuit voltage, I_{sc} is the short circuit current, R_i is the internal resistance of the generator, and P_{max} is the maximum power output.

APPENDIX B.--LIST OF SYMBOLS

a	Inner radius of generator
b	Outer radius of generator
$\vec{B}$	Magnetic flux density
B_o	Flux density of applied magnetic field
e	Electron charge
$\vec{E}$	Electric field
I	Total current
I_{sc}	Short circuit current
$\vec{J}$	Current density
L	Length of generator
N_e	Electron density
P	Pressure
P_{max}	Maximum power output
r	Radial coordinate
R_1	Internal resistance of generator
R_L	External load resistance
$\vec{U}$	Gas velocity
$U_\theta^\circ(r)$	Inlet tangential velocity profile
z	Axial coordinate
β	$\frac{1}{eN_e}$
θ	Angular coordinate
V	Terminal voltage
V_o	Open circuit terminal voltage
ρ	Gas density
σ	Scalar conductivity
σ'	$\frac{\sigma}{1 + (\sigma \beta B_o)^2}$

INT.-BU.OF MINES,PGH.,PA. 18006